Northumbria
University
NEWCASTLE

A Strategy for Modelling Mechanochemically Induced Unzipping and Scission of Chemical Bonds in Double-Network Polymer Composite

Haibao Lu[a,*], Xiaojuan Shi[a], Kai Yu[b] and Yong Qing Fu[c]

[a]Science and Technology on Advanced Composites in Special Environments Laboratory, Harbin Institute of Technology, Harbin 150080, China

[b]Department of Mechanical Engineering, University of Colorado Denver, Denver, CO 80217, United States

[c]Faculty of Engineering and Environment, Northumbria University, Newcastle upon Tyne, NE1 8ST, UK

[*]E-mail: luhb@hit.edu.cn (H. Lu)

Abstract: A molecular mechanics model for covalent and ionic double-network polymer composites was developed in this study to investigate mechanisms of mechanochemically induced unzipping and scission of chemical bonds. Morse potential function was firstly applied to investigate mechanical unzipping of the covalent bonds, and then stress-dependent mechanical energy for the interatomic covalent bonds was discussed. A new mechanochemical model was formulated for describing the mechanically induced ionic bond scissions based on the Morse potential model and equations for electrostatic forces. Based on this newly proposed model, mechanochemical behaviors of several common interatomic interaction types (e.g., $A^{+}B^{-}$, $A^{2+}B^{2-}$/$A^{2+}2B^{-}$/$2A^{+}B^{2-}$ and $A^{3+}B^{3-}$/$A^{3+}3B^{-}$/$3A^{+}B^{3-}$) of the ionic bonds have been quantitatively described and analyzed. Finally, mechanochemical unzipping of the covalent bonds and dissociation of the ionic bonds have been characterized and analyzed based on the molecular mechanics model, which has well predicted the chemical and mechanochemical activations in the covalent and ionic double-network polymer

composites.

Keywords: mechanochemical; molecular mechanics; modelling; bond scission; double-network polymer

1. Introduction

Understanding the chemical responses of polymers to mechanical loading are crucial for wide-range research areas in polymer science and technology, as well as for designs of new types of stress-responsive and energy-transduction polymers [1-3]. Mechanical loading, i.e., using high pressure, mechanical forces or ultrasound [4-6], provides an effective stimulus approach for chemists to design/fabricate novel materials [7-9], similar to those using heat, light or electricity [10-12]. Various types of stress-responsive and energy-transduction polymers have been produced based on the chemical reactions of molecule bonds in response to the external stresses or forces, including flow-induced mechanochemistry of polymers in solution [13], mechanically-induced dichroism [14,15] and ultrasonication-induced chain scissions in polymers [16]. These mechanochemical processes in polymers have attracted great attention due to their special constitutive relationships and significant changes in properties. However, currently there are few models or constitutive equations available to describe the working mechanisms (or theoretical and experimental principles) and constitutive relationships for the mechanochemical behaviors of polymers [17-19]. There is no special theory which could be used to explain the experimental results and explore the fundamental mechanisms, thus resulting in the theoretical studies seriously lagged behind the experimental ones. Clearly, it is crucial to develop theoretical models for the mechanochemical activations in the polymers and provide a guidance for further design and

optimization of the next generation polymers.

Conventional hydrogels are composed of a single network of hydrophilic polymers. They usually break at a tensile stress less than sub-MPa and a strain less than 100% [20,21]. Their mechanical properties have been regarded as soft and weak [21]. For this reason, interpenetrating but independently cross-linked double network (DN) hydrogels have been developed to improve the mechanical strength [20-23]. These DN hydrogels, which are highly stretchable and tough, have been considered as the potential metamaterials for robot, medicine and aerospace [20-23]. A high content of water molecules and improved mechanical strength and toughness have been achieved in the DN hydrogels [22,23]. However, the enhancing mechanisms of mechanical properties of the DN hydrogels are different from those general ones for enhancing the toughness of soft polymeric materials. It was demonstrated that the improved strength and toughness are originated from the local yielding mechanism to resist the externally mechanical loading [24]. Therefore, the constitutive relationships of the DN hydrogels present an interesting but challenging issue in the modeling and simulation of their mechanical behaviors.

Previously, several theoretical models have been proposed to study and characterize the mechanochemical behavior of the DN hydrogels [25-28]. However, chemical and mechanochemical activations have not been considered or modeled in those previous studies, and only mechanical behaviors of the DN hydrogels have been investigated according to mechanical testing results. Therefore, it is critical to develop a new model for exploring the chemical and mechanochemical activations and the working mechanisms of the mechanochemical behaviors of the DN hydrogels.

In this study, a molecular mechanics model was proposed based on the Morse potential function model by combining the influences of bond unzipping and scission for the DN hydrogel. The Morse potential function was initially employed to investigate the mechanical unzipping of covalent bonds. Meanwhile, a mechanochemical model was formulated for the mechanically induced scissions of ionic bonds according to the Morse potential function model and electrostatic force equation. The mechanical behaviors of several interatomic interaction types of the ionic bonds have been quantitatively analyzed and discussed. Finally, the mechanochemically induced covalent-bond stretching and ionic-bond dissociation have been characterized and analyzed using the molecular mechanics model to predict the chemical or mechanochemical activation in the DN hydrogel/polymer.

2. Morse potential function of mechanochemical unzipping for covalent network

Interatomic interaction of a covalent bond is represented by the Morse potential theory, and the interatomic potential ($U(x)$) is presented as [29]:

$$\frac{U(x)}{D_c} = 1 - \left[\exp(-2\alpha x) - 2\exp(-\alpha x)\right] \quad (1)$$

where D_c is the dissociation energy of the interatomic covalent bond without vibrations, α is the Morse coefficient and x is the distance of the interatomic bond [30]. The function $U(x)$ is linked to the Morse potential of the covalent bond as a function of bond distance x. However, if the bond is under a constant tension force f_U applied to either of its ends, the activation energy required to break the bond is diminished from D_c to $U(x)$. A schematic illustration for the distance of interatomic bonds under a constant force is presented in Figure 1. When the covalent bond is stretched with the force per unit area $f_U > 0$, the distance of interatomic covalent bond is increased from x to $x + \Delta x$. The variation of the activation

energy for disassociation of the bond under a force of f_U is given by [31],

$$\frac{U(f_U)}{D_c} = \sqrt{1-\frac{f_U}{F_m}} - \frac{f_U}{2F_m}\ln\frac{1+\sqrt{1-\frac{f_U}{F_m}}}{1-\sqrt{1-\frac{f_U}{F_m}}} \tag{2}$$

where F_m is the ultimate strength of the bond. The function $U(f_U)$ shows the variations of the Morse potential of the covalent bond as a function of tensile force. Equation (2), which describes the conversion of mechanical energy into chemical one, can be used to account for the dissociation of mechanically strained bonds. Both the equations (1) and (2) are originated from the Morse potential function model, and they present the constitutive relationships for the mechanical energy with the interatomic bond distance (x) and stress f_U for the covalent network. When a chemical bond of the covalent network is extended before bond breaking, its energy diminishes. At the equilibrium condition, the deformation energy of the covalent bond can be written as [32]:

$$U_{\text{def}} = \int_{r^0}^{r} f_U dr = \int_{V^0}^{V} \sigma_U dV \tag{3}$$

where f_U and σ_U are the force and stress applied on the bond, r_0 and r are the lengths of the initial and deformed bonds, while V_0 and V are the corresponding activation volumes.

[Figure 1]

Here, a constant tensile force (f_U) is applied, and leads to a change in the Morse potential and deformation of the chemical bond. The mechanical energy can thus be expressed as:

$$W_m = U(f_U) + U_{\text{def}} \tag{4}$$

It is assumed that the isotropic covalent network is under a constant tensile force (f_U), thus, the mechanical energy can be given by,

$$W_m = D_c\left\{1-\left[2\exp(-\alpha x)-\exp(-2\alpha x)\right]\right\}+\int_{r^0}^{r} f_U dr \quad (5)$$

Here, we introduce a dimensionless force $P=\frac{f_U}{F_m}$ ($0\le P\le 1$), where $F_m = D_c\frac{\alpha}{2}$ is the maximum force under a static elastic tension of the bond according to the condition $d^2U(x)/dx^2=0$ [29]. Therefore, equation (5) can be rewritten as:

$$W_m = D_c\left\{1-\left[2\exp(-\alpha x)-\exp(-2\alpha x)\right]\right\}+D_c\cdot\frac{P}{2}(\alpha x) \quad (6)$$

The values of the bond elongation and interatomic force are related to the mechanical energy for the deformation (or rupture) of the covalent bonds. It is necessary to study the dependence of mechanical energy on the bond elongation, which has a crucial role in determining the interatomic force. The evolution curves of the mechanical energy (W_m/D_c) as a function of bond elongation (x) with a given constant Morse coefficient (α) and dimensionless force (P) are presented in Figure 2. When the bond is stressed, it is found that the Morse potential is gradually decreased while the mechanical energy is increased with an increase in the bond elongation. As shown in Figure 2(a), the mechanical energy for the covalent bond stretching is increased with an increase in the Morse coefficient (α) at the same bond elongation. If the Morse coefficient (α) is assumed to link directly to the bond number (which is defined as the number of the chemical bonds in a covalent network). More mechanical energy is necessary to stretch the covalent bonds to a given elongation due to the increase in the bond number and the value of αx. On the other hand, the mechanical energy is also gradually increased with an increase in the applied force (e.g., the dimensionless force P) at a constant Morse coefficient (α) due to the increase in the mechanical energy for deformation, where the Morse potential of the bond is kept a constant as presented in Figure

2(b). These results clearly show that the mechanical energy of the covalent bonds is determined by the bond elongation, bond number (Morse potential constant) and the applied force.

[Figure 2]

According to equation (6), a constitutive relationship between the force per unit area and displacement over the initial distance of the covalent bond can be written as,

$$S_{\mathrm{m}} = \frac{\partial(W_{\mathrm{m}})}{\partial x} = \alpha \cdot D_c \cdot \left[2\exp(-\alpha x) - 2\exp(-2\alpha x) + \frac{P}{2} \right] \tag{7}$$

Figures 3(a) and 3(b) plot the constitutive relationships of the stress function and bond elongation function for the covalent bonds. For a given Morse coefficient, e.g., $\alpha = 10^{10}$, 2×10^{10}, 3×10^{10}, 4×10^{10} or 5×10^{10}, it is found that the force per unit area gradually increases when the displacement over the initial distance of the covalent bond is increased from 0 to 0.68×10^{-10}m, 0.36×10^{-10}m, 0.24×10^{-10}m, 0.17×10^{-10}m or 0.14×10^{-10}m, respectively, as shown in Figure 3(a). However, it becomes decreasing with the further increase in the bond elongation. This indicates that the inter-atomic force per unit area among the covalent bonds is initially increased and then decreased with the gradual increase in the bond elongation.

Dependence of the normalized stress on the force per unit area of the covalent bond is shown in Figure 3(b). It reveals that the mechanical force is gradually increased with an increase in the external applied stress, where the bond elongation reaches to a constant value. It indicates that the externally applied force has a strong influence on the force per unit area of the covalent bonds, as they have been stretched to a constant bond elongation.

[Figure 3]

3. Modelling of mechanochemically induced scissions of ionic bonds

The Morse potential was used for the covalent bonds in the above section under a mechanical loading. Whereas the mechanochemical behavior of the ionic bond is different from that of the covalent bond as the bonds will be broken under a large force. It is necessary to consider the electrostatic force for the ionic bond, in which the cationic and anionic groups have interactively attractive forces resulted from the mechanochemically induced bond scissions [33]. However, there was no previous work considering this in modelling and simulation.

Under a mechanical loading applied to the ionic bond (only an axially tensile force is considered and discussed in this study), the cationic and anionic groups have the polarization interactions after the ionic bonds have been dissociated and then they are separated from each other. There are dipolar and intermolecular forces resulted from the electrostatic forces among the cationic and anionic groups. These inter-molecular forces are able to resist the external loading and have a following constitutive relationship with the spatial distance of the cationic and anionic groups [33].

$$F_p = k\left(-\frac{e^2}{R}+\frac{e^2}{R-l_1}+\frac{e^2}{R+l_2}-\frac{e^2}{R+l_2-l_1}\right) \tag{8}$$

where k (k=9×10^{9}N·m^2/C^2) is the electrostatic constant, e (e=1.6×10^{-19}C) is the elementary charge. R is the end-to-end distance of two groups, and l_1 and l_2 are the lengths of the two groups along the axial force. It is assumed that $l_1 = l_2 = r$ and $x = R - r$ in this study. Therefore, the equation (8) can be rewritten as,

$$F_p = k\left(-2\frac{e^2}{R}+\frac{e^2}{R-r}+\frac{e^2}{R+r}\right) \tag{9}$$

Here it is necessary to determine the boundary conditions for the electrostatic force as it begins dominant after the bond scission. To determine the initial boundary of the R_0, the static elastic tension (F_m) of the bond is needed in order to describe the ionic bond scission, which has been ruptured by means of the mechanical force. Therefore, dimensionless forces are introduced: P=1 and $F_m = D_i \frac{\alpha_i}{2}$ [33], in which D_i is the dissociation energy and α_i is the coefficient in the Morse expression of the interatomic ionic bond. There is a conversion of mechanical into chemical energy in the process of the ionic bond scission, e.g., $U_{def} = D_i \Rightarrow F_m \cdot (R_0 - r) = D_i$ and $R_0 = \frac{2}{\alpha_i} + r$. Therefore, the boundary of the R is ranged from ($R_0 = \frac{2}{\alpha_i} + r$) to ($R$). The mechanical energy to resist the electrostatic force of an ionic bond can then be presented as:

$$W_e = \int_{R_0}^{R} F_p d(x) = \int_{R_0}^{R} k \cdot \left(-2\frac{e^2}{R} + \frac{e^2}{R-r} + \frac{e^2}{R+r} \right) d\left[(R-r) \right] \tag{10}$$

Thus,

$$W_e = k \cdot e^2 \cdot \left(-\ln \frac{R^2}{R^2 - r^2} + \ln \frac{R_0^2}{R_0^2 - r^2} \right) \quad \left(\text{where } R_0 = \frac{2}{\alpha_i} + r \right) \tag{11}$$

According to equation (11), the electrostatic force among cationic and anionic groups is gradually decreased with the increase in the mechanically induced scissions. However, the mechanical energy to resist the increase in electrostatic force is gradually increased as shown in Figure 4(a). It increases sharply at the initial elongation of the ionic bonds, but then the increase rate decreases as the strength of electrostatic force is decreased. Furthermore, the mechanical energy is increased when the value of R_0 is decreased from 1.5*r*, 1.4*r*, 1.25*r* to 1.2*r*. These simulation results reveal that the elongation of the ionic bond has a strong effect

on both the electrostatic force and mechanical energy.

Figure 4(b) depicts the relationship between the mechanical energy of the ionic bond and Morse potential constant, according to the equation (11). For different values of R/r=1.01, 1.05, 1.2 and 2.0, the mechanical energy to resist the electrostatic force of the ionic bond increases gradually with the increase of Morse potential constant. If the Morse potential constant is assumed to be the bond number, the mechanical energy is gradually increased with the increase of the bond number as each bond is stretched to a constant elongation of R/r=1.01, 1.05, 1.2 and 2.0. Results clearly show that the bond number also plays a critical role to influence the mechanical energy and resist the electrostatic force even after the mechanically induced scissions of these ionic bonds.

[Figure 4]

However, equation (11) only presents the electrostatic interaction for the ionic bond of A^+B^- type, of which the cationic group has the same electric charge with that of the anionic group. It is necessary to characterize the electrostatic interactions of the ionic bond types of $A^{2+}2B^-$ (or $2A^+B^{2-}$) and $A^{3+}3B^-$ (or $3A^+B^{3-}$), in order to separate the effects of electric charge on the electrostatic interaction of the cationic group (or groups) and anionic group (or groups). Figures 5(a) and 5(b) present the electrostatic interactions for the $A^{2+}2B^-$ (or $2A^+B^{2-}$) and $A^{3+}3B^-$ (or $3A^+B^{3-}$) ionic bonds, respectively, under an axial tensile force. It is found that the electrostatic interaction of the $A^{2+}2B^-$ (or $2A^+B^{2-}$) bond is same with that of the $A^{2+}B^{2-}$ bond along the axial direction, as their bond elongations are kept a constant. While the electrostatic interaction of the $A^{3+}3B^-$ (or $3A^+B^{3-}$) bond is same with that of the $A^{3+}B^{3-}$ bond along the axial direction. Clearly, the electrostatic interaction force is only determined by the distance

of the cationic and anionic groups along the axial direction.

[Figure 5]

The electrostatic force of the mechanically induced scissions of the $A^{2+}2B^{-}$ (or $2A^{+}B^{2-}$) ionic bond and $A^{3+}3B^{-}$ (or $3A^{+}B^{3-}$) ionic bond can now be presented as,

$$\begin{cases} F_p = k\left(-2\dfrac{(2e)^2}{R}+\dfrac{(2e)^2}{R-r}+\dfrac{(2e)^2}{R+r}\right)=4k\left(-2\dfrac{e^2}{R}+\dfrac{e^2}{R-r}+\dfrac{e^2}{R+r}\right) \\ F_p = k\left(-2\dfrac{(3e)^2}{R}+\dfrac{(3e)^2}{R-r}+\dfrac{(3e)^2}{R+r}\right)=9k\left(-2\dfrac{e^2}{R}+\dfrac{e^2}{R-r}+\dfrac{e^2}{R+r}\right) \end{cases} \tag{12}$$

According to equation (12), the mechanical energy that is needed to resist the electrostatic force is given below,

$$\begin{cases} W_e = 4k\cdot e^2\cdot\left(-\ln\dfrac{R^2}{R^2-r^2}+\ln\dfrac{R_0^2}{R_0^2-r^2}\right) \quad \left(\text{where } R_0=\dfrac{2}{\alpha_i}+r\right) \\ W_e = 9k\cdot e^2\cdot\left(-\ln\dfrac{R^2}{R^2-r^2}+\ln\dfrac{R_0^2}{R_0^2-r^2}\right) \quad \left(\text{where } R_0=\dfrac{2}{\alpha_i}+r\right) \end{cases} \tag{13}$$

Figures 6(a) and 6(b) present the numerical results of the mechanical energy to resist the electrostatic forces for the $A^{+}B^{-}$, $A^{2+}B^{2-}$ ($A^{2+}2B^{-}$ or $2A^{+}B^{2-}$) and $A^{3+}B^{3-}$ ($A^{3+}3B^{-}$ or $3A^{+}B^{3-}$) ionic bonds as a function of elongation of the ionic bond and Morse potential constant, respectively. These simulation results reveal that the quantities of electric charges of the cationic or anionic groups have critical roles in determining the mechanical energy to resist to the electrostatic force, e.g., the mechanical energy is increased with an increase in the quantities of electric charges. It should be noted that the electrostatic force of the $A^{2+}B^{2-}$ bond is the same with that of the $A^{2+}2B^{-}$ or $2A^{+}B^{2-}$ bond under the axial force while the repulsive forces of the B^{-} and B^{-} groups in $A^{2+}2B^{-}$ bond (or A^{+} and A^{+} groups in $2A^{+}B^{2-}$ bond) are different from that of $A^{2+}B^{2-}$ bond. This is because the vertically repulsive force has no

apparent effect on the elongation of the bond along the axial direction.

[Figure 6]

4. Modelling of the mechanical performance of double-network polymer composite

For the DN polymer that is incorporated of a covalent network (made from m covalent bonds) and an ionic network (made from n ionic bonds), the mechanical energy (W) of the tensile force applied on the polymer is resulted from both networks, i.e.,

$$\begin{cases} W = mW_m + nW_i \\ W_i = W_e + D_i \\ W_m = D_c\left\{1-\left[2\exp(-\alpha x)-\exp(-2\alpha x)\right]\right\} + D_c \cdot \dfrac{P}{2}(\alpha x) \\ W_e = k \cdot e^2 \cdot \left(-\ln\dfrac{R^2}{R^2-r^2} + \ln\dfrac{R_0^2}{R_0^2-r^2}\right) \quad \left(\text{where } R_0 = r + \dfrac{2}{\alpha} \text{ and } x = R-r\right) \end{cases} \tag{14}$$

where W_m and W_i are the mechanical energy values for the covalent network and ionic network, respectively; D_c and D_i are the dissociation energy values of the covalent network and ionic network, respectively. When the Morse potential function is initially introduced, the vibration of the polymer chain has not been considered. Therefore, the effect of entropic change on the mechanical energy has not been considered. For the thermodynamic of polymer, the entropy function should be considered as the vibrational energy plays a critical role in determining the free-energy ($W = U - TS + pV$). However, the stretching (λ) of the polymer is generally applied to describe the entropy change for the rubbery polymer. Similar to the rubbery network polymer, for the double-network polymer, the bond is stretched when the force is applied, and the bond will be recovered with the external force removed. According to the Flory-Huggins theory [27], the free-energy of a stretched network of polymers can be written as $W_s = \dfrac{3}{2}NkT\left(\lambda^2 - 1 - 2\log\lambda\right)$, where N is the number of chains, k is the Boltzmann's constant and T is the temperature.

The mechanical energy of the tensile force can be rewritten as,

$$W = m\left\{D_c\left\{1-\left[2\exp(-\alpha x)-\exp(-2\alpha x)\right]\right\}+D_c\cdot\frac{P}{2}(\alpha x)\right\} + n\left\{k\cdot e^2\cdot\left(-\ln\frac{R^2}{R^2-r^2}+\ln\frac{R_0^2}{R_0^2-r^2}\right)+D_i\right\} \quad (15)$$

The values of D_c and D_i are constants when the covalent and ionic networks are fixed. It is assumed that $D_i \approx 0$ (e.g., energy dissipation is not considered in this part). Therefore, the following expression is obtained in this study,

$$W = m\cdot D_c\cdot\left\{\left\{1-\left[2\exp(-\alpha x)-\exp(-2\alpha x)\right]\right\}+\frac{P}{2}(\alpha x)\right\} + n\left\{k\cdot e^2\cdot\left(-\ln\frac{R^2}{R^2-r^2}+\ln\frac{R_0^2}{R_0^2-r^2}\right)\right\} \quad (16)$$

It is assumed that $r = 10^{-10}$m for both the covalent bond and ionic bond, and $n/m = \alpha = 10^{10}$, 1.25×10^{10}, 1.6×10^{10} or 2×10^{10}. If the covalent network has not been broken, its mechanical performance could be characterized by assuming it is a covalent bond. Whereas if the ionic network is broken under the mechanical force, its bond number is assumed to be same value of the Morse potential constant, $D_c = \frac{1}{N_A}\cdot$ 301kJ/mol$=5\times10^{-19}$J ($N_A = 6.02\times10^{23}$, is the Avogadro constant) [33], $k = 9\times10^9$N$\cdot$m^2/C^2, $e = 1.6\times10^{-19}$C, $P = 0.4$. Thus, equation (16) can be further modified as,

$$W = D_c\cdot\left\{\left\{1-\left[2\exp(-\alpha x)-\exp(-2\alpha x)\right]\right\}+\frac{P}{2}(\alpha x)\right\} + \alpha\cdot\left\{k\cdot e^2\cdot\left(-\ln\frac{R^2}{R^2-r^2}+\ln\frac{R_0^2}{R_0^2-r^2}\right)\right\} \quad (17)$$

[Figure 7]

Equation (17) presents a constitutive relationship between the mechanical energy as a function of the bond elongation x (it is assumed that the bond elongation of covalent is

same with that of the ionic bond, e.g., $x_c = x_i = x$) as shown in Figures 7(a), 7(b), 7(c) and 7(d) at the given ionic bond numbers of $\alpha = 10^{10}$, 1.25×10^{10}, 1.6×10^{10} or 2×10^{10}, respectively. Both the polar and deformation mechanical energy values are gradually increased with the increase in the bond elongation. The simulation results confirm that the polar mechanical-energy also plays an essential role to resist the externally mechanical loading, and this polar mechanical-energy is resulted from the electrostatic interactions of the cationic group with the anionic groups. If the mechanically induced scission of the ionic bonds happens, the cationic or anionic groups start to resist the externally mechanical loading through changes of their electrostatic forces. Therefore, the mechanical energy that is necessary to deform the covalent bonds and resist the electrostatic forces of the ionic bonds becomes a function of the ionic bond elongation as shown in Figure 8(a). With the bond number increased from $\alpha = 10^{10}$, 1.25×10^{10}, 1.6×10^{10} to 2×10^{10}, more mechanical energy is needed to stretch the ionic bonds to a given bond elongation. While the bond number function (α) has no apparent effect on the mechanical energy applied on the covalent bond, of which the bond elongation is kept a constant under the stretching force. Furthermore, the effect of the bond number on the mechanical energy applied on the ionic bonds has been studied and characterized, with the results shown in Figure 8(b). It is found that much more mechanical energy should be applied on the ionic bonds with an increase in the bond number from $\alpha = 10^{10}$, 1.25×10^{10}, 1.6×10^{10} to 2×10^{10}, which is resulted from the increased elongation of the ionic bonds (αx).

[Figure 8]

Furthermore, Figure 9 presents changes of the mechanical energy as a function of the

covalent (or ionic) bond elongation at given ionic bond numbers of $\alpha=10^{10}$, $\alpha=1.25\times10^{10}$, $\alpha=1.6\times10^{10}$ and $\alpha=2\times10^{10}$. Simulation result reveals that the mechanical energy used to resist the electrostatic force from the ionic bonds is increased with the increase of bond numbers. It well agrees with the previously reported studies that the free energy is much higher for the polymer with a higher concentration of the ions [28]. Therefore, the amount of the polar mechanical-energy becomes larger as more mechanical energy is applied on the covalent and ionic bonds, thus resulting in an increased value of the polar mechanical-energy and large divergence of the deformation mechanical-energy. This simulation result helps to separate the effect of the mechanical energy applied on the ionic bonds from that on the covalent bond. However, it is necessary to consider the electrostatic force resulted from ionic bond scission in the modeling and simulation of the DN polymers.

[Figure 9]

By comparing equations (7) with (17), the deviatoric part of the stress function can be described as,

$$\begin{cases} S_m = \dfrac{\partial(W_{\mathrm{m}})}{\partial x} = \alpha_c \cdot D \cdot \left[2\exp(-\alpha_c x) - 2\exp(-2\alpha_c x) + \dfrac{P}{2} \right] \\ S_i = \dfrac{\partial(W_{\mathrm{i}})}{\partial x} = F_p = k\left(-2\dfrac{e^2}{R} + \dfrac{e^2}{R-r} + \dfrac{e^2}{R+r} \right) \end{cases} \tag{18}$$

where S_m and S_i are the forces per unit area for the covalent and ionic bonds, respectively. α_c is the Morse potential constant of the covalent bond.

In the double-network polymer composite, it is generally assumed that mechanically induced scission will happen in the ionic bonds at the beginning state of deformation to resist the external mechanical force. Here, it is assumed that the dissociation energy of the ionic network has no apparent effect on the stress function of the polymer. Accordingly, equation

(18) could be expressed as follows:

$$\begin{cases} S = S_m \quad (R < R_0) \\ = \alpha_c \cdot D_c \cdot \left[2\exp(-\alpha_c x) - 2\exp(-2\alpha_c x) + \dfrac{P_c}{2} \right] \\ S = S_m + F_p \quad (R \geq R_0) \\ = \alpha_c \cdot D_c \cdot \left[2\exp(-\alpha_c x) - 2\exp(-2\alpha_c x) + \dfrac{P_c}{2} \right] + \alpha_i \cdot k \left(-2\dfrac{e^2}{R} + \dfrac{e^2}{R-r} + \dfrac{e^2}{R+r} \right) \end{cases} \tag{19}$$

where S is the force per unit area of the double-network polymer composite, and α_i is the Morse potential constant of the ionic network. After the ionic bond scission is induced by the external force, the electrostatic force begins to influence the stress function. According to results obtained from equation (19), Figure 10 plots the constitutive curves of the forces as a function of elongation of covalent (or ionic) bond at the given Morse potential constants of $\alpha_i = \alpha_c = 10^{10}$, $\alpha_i = \alpha_c = 1.25\times10^{10}$, $\alpha_i = \alpha_c = 1.6\times10^{10}$ and $\alpha_i = \alpha_c = 2\times10^{10}$. Results show that the force applied on the double-network polymer composite is sharply increased when the displacements over the initial distance of the bonds are decreased from $x = 2.0\times10^{-10}$m, $x = 1.6\times10^{-10}$m, $x = 1.125\times10^{-10}$m and $x = 1.0\times10^{-10}$m, respectively, which is mainly resulted from combined actions from both the mechanically induced scission and electrostatic force of the ionic bonds. A large amount of the mechanical energy is dissipated for breaking the ionic bonds, whereas there is no apparent change in the bond elongation. That is to say, a large amount of the mechanical energy is transformed into the chemical energy for the ionic bond scission.

[Figure 10]

However, it is necessary to characterize the mechanical behavior of the ionic bonds before they are mechanically deformed to induce scission. Here it is assumed that the mechanical

behavior of the ionic bonds can also be described using the Morse potential expression before they are broken, i.e.,

$$\frac{U(x)}{D_i} = 1 - \left[\exp(-2\alpha_i x) - 2\exp(-\alpha_i x)\right] \tag{20}$$

where D_i is the dissociation energy of the interatomic ionic bond without any vibrations, α_i is the coefficient in the Morse expression (α_i is also assumed to the bond number of the ionic network) [34] and x is the distance of the interatomic bond. Before the ionic bonds are broken, the electrostatic force of the ionic bonds is a sum of that of each ionic bond due to their homogeneous and uniform mechanical property. In the case of the breaking of ionic bonds, an equilibrium equation can be obtained according to the Morse potential equation and electrostatic force equation as following,

$$D_i \cdot \left[2\exp(-\alpha_i x_0) - 2\exp(-2\alpha_i x_0) + \frac{P_i}{2}\right] = \alpha_i \cdot k\left(-2\frac{e^2}{R_0} + \frac{e^2}{R_0 - r} + \frac{e^2}{R_0 + r}\right) \left(R_0 = r + \frac{2}{\alpha_i},\ x_0 = \frac{2}{\alpha_i}\right) \tag{21}$$

Thus, the dissociation energy function of the ionic bond could be expressed as,

$$D_i = \frac{\alpha_i \cdot k\left(-2\frac{e^2}{R_0} + \frac{e^2}{R_0 - r} + \frac{e^2}{R_0 + r}\right)}{\left[2\exp(-\alpha_i x_0) - 2\exp(-2\alpha_i x_0) + \frac{P_i}{2}\right]} \tag{22}$$

When there is mechanically induced scission in the ionic bond, P_i =1.

According to $F_m = D_i \frac{\alpha_i}{2}$, the maximum force under a static elastic tension of the ionic bond is presented as,

$$F_m = D_i \frac{\alpha_i}{2} = \frac{\alpha_i \cdot k\left(-2\frac{e^2}{R_0} + \frac{e^2}{R_0 - r} + \frac{e^2}{R_0 + r}\right)}{\left[2\exp(-\alpha_i x_0) - 2\exp(-2\alpha_i x_0) + \frac{P_i}{2}\right]} \cdot \frac{\alpha_i}{2} \tag{23}$$

Equations (22) and (23) show the constitutive relationships between the dissociation energy (D_i) and maximum force (F_m) for the ionic bonds. As the bond number is gradually increased, both the dissociation energy (D_i) and maximum force (F_m) of the interatomic ionic bond are increased as shown in Figures 11(a) and 11(b). The simulation results reveal that both the dissociation energy and maximum force under a static elastic tension are essentially determined by the bond number of the ionic network, e.g., higher stress and mechanical energy are needed to apply on the ionic network for the bond dissociation as more ionic bonds are incorporated into the network. It is well known that the active energy of the polymer chain is increased with the increase of monomer numbers according to the thermodynamics of polymers [34]. With an increase in the active energy, a high mechanical energy should be provided in order to maintain a constant stretching ratio. The working mechanism of the monomer number on the active energy is similar to that of bond number on the mechanical energy of the ionic network.

[Figure 11]

However, there are mechanically induced scissions of the ionic bonds generated to resist the external mechanical force. It is difficult to characterize the mechanical behavior of the ionic bonds in the DN polymer during their stretching, which would be similar to that of the covalent bonds. Therefore, the Morse potential function is again used to depict the mechanically induced stretching of the ionic bonds before their dissociation. Here, the equation (20) can be expressed as follows,

$$\begin{cases} S_t = S_c + S_i \quad (R < R_0) \\ = \alpha_c \cdot D_c \cdot \left[2\exp(-\alpha_c x) - 2\exp(-2\alpha_c x) + \frac{P_c}{2} \right] + \alpha_i \cdot D_i \cdot \left[2\exp(-\alpha_i x) - 2\exp(-2\alpha_i x) + \frac{P_i}{2} \right] \\ S_t = S_c + F_p \quad (R \geq R_0) \\ = \alpha_c \cdot D_c \cdot \left[2\exp(-\alpha_c x) - 2\exp(-2\alpha_c x) + \frac{P_c}{2} \right] + \alpha_i \cdot k \left(-2\frac{e^2}{R} + \frac{e^2}{R-r} + \frac{e^2}{R+r} \right) \end{cases} \quad (24)$$

According to equation (24), the covalent bonds will be stretched to resist the external mechanical force according to the Morse potential function. It reveals that the ionic bonds are stretched to resist the external mechanical force, and then the electrostatic forces are activated before and after they are broken. Therefore, the constitutive relationship between the force per unit area and displacement over the initial distance could be able to describe the mechanochemical behavior of the DN polymer. Figure 12 plots the simulation curves for the mechanical force as a function of the covalent (or ionic) bond elongation at different Morse potential constants of $\alpha_i = \alpha_c$ =10^{10}, $\alpha_i = \alpha_c$ =1.25×10^{10}, $\alpha_i = \alpha_c$ =1.6×10^{10} and $\alpha_i = \alpha_c$=2×10^{10}. It is revealed that there is a distinct difference of the mechanical forces for the covalent network and DN as shown in Figures 12(a) and 12(c). The maximum differences of the mechanical forces reach to 56.67%, 67.54%, 80.52% and 83.38%, respectively, at different Morse potential constants of $\alpha_i = \alpha_c$ =10^{10}, $\alpha_i = \alpha_c$ =1.25×10^{10}, $\alpha_i = \alpha_c$ =1.6×10^{10} and $\alpha_i = \alpha_c$ =2×10^{10} as presented in Figures 12(b) and 12(d). These simulation results clearly show that the mechanical force applied on the ionic bonds is significantly increased with an increase in the bond number. Therefore, large differences of the mechanical forces have been found between the covalent and DN network.

[Figure 12]

5. Verification approaches of theoretical results

From an experimental perspective, measurement of the elongation of a covalent bond x is quite challenging, owing to the nature of the resonant frequency of vibration. At the same time, the mechanical failure of the bulk material is rather a complex process, and the number of bonds rupturing at a given time, their angular distribution, and the role of shear forces and friction are difficult to be assessed. Therefore, it remains a great challenge to correlate the mechanical properties determined from the bulk material to those of the individual chemical bonds. Newly developed single-molecule techniques generally based on the atomic force microscope (AFM) [35] have been developed for the measurement of the mechanical properties of individual molecule and bond directly. Owing to the simplicity of this approach, a vast number of natural and synthetic molecules and their bonds can be studied using a single-molecule force spectroscope.

The AFM was developed to directly measure the force to generate of a chemical bond [36], and also generate atomically resolved images of surfaces with characteristic features and defects [37-39]. These truly atomic-scale contrast images are resulted from the short range chemical interactions between an atomically sharp AFM tip and the nearest atoms on the surface of the sample. In principle, it maps the potential of chemical bonding between the foremost atoms on an AFM tip. The separation of the tip and substrate can be employed for the elongation of the chemical bonds. Therefore, the modeling results could be verified based on the experimental ones from the AFM measurement.

The force-distance and interaction energy-distance relations of a single covalent bond are initially measured by the AFM, respectively. To determine the elongation of a covalent bond

over which only the AFM forces are acting, sphere-plane model or first-principles calculation is necessary to be used to fit the experimental data. Furthermore, the energy-force relation for the interaction is also calculated from the force-distance and interaction energy-distance relations of a single covalent bond. According to the experimental data determined by the AFM, the simulation results of the mechanochemically induced covalent bond could be compared for verification as shown in Figure 13. Figure 13(a) plots the numerical results for the mechanical energy as a function of the elongation (x), and the experimental data are also plotted for comparisons. It is found that the difference of the simulation and experimental results is within 80%, as revealed in Figure 13(b). Meanwhile, Figure 13(c) plots the numerical results for the stress as a function of the elongation (x). and the difference of the simulation and experimental results is within 50%, as revealed in Figure 13(d). It is found that the theoretical simulation results are in good agreements with the experimental ones. This shows that the modelling results could be verified by the AFM results.

Mechanically induced scission of covalent bonds has previously been experimental investigated using AFM analysis [40]. Infrared (IR) spectroscopy was generally used for the investigation of polymer degradation. The infrared method was also used for the measurements of terminal groups formed as a result of macromolecular degradation in specimens fractured under uniaxial tension [41]. The spectrometer recorded the difference in absorption of the undeformed and fractured specimens ($\Delta D = D - D_0$, where is D_0 the dissociation energy of undeformed bond, D the dissociation energy of fractured bond). The scission of the ionic bonds can be determined using the IR spectroscopy as well. However, the experimental measurement of the scission of ionic bond has never been reported using the

IR measurement. After the rupture of the ionic bond, the AFM method can then be employed to measure the force and elongation of the ruptured ionic bond. In this way, the modeling results may potentially be validated by the experimental data in the future work.

6. Conclusion

In this study, we proposed a molecular mechanics framework to study the mechanically induced stretching and bond scission of the double-network polymer composite based on the Morse potential function model and electrostatic force equations. We have demonstrated that the proposed constitutive framework is able to predict mechanical and chemical transitions and their mechanochemical behavior of the double-network polymer composite. This proposed constitutive framework provides an effective approach to quantitatively analyze the dependence of mechanochemical behavior on the applied stress, covalent (or ionic) bond elongation, Morse potential constant and bond numbers of the double-network. The working mechanism in the mechanochemically induced bond stretching and scission has been identified and the constitutive relationship is obtained. The contribution of the ionic bonds to the mechanical properties has been systemically studied, as the ionic bonds resist the applied stress by means of mechanical stretching, bond dissociation and electrostatic interaction. Furthermore, the mechanochemical behaviors of several classical interatomic interaction types ($A^{+}B^{-}$, $A^{2+}B^{2-}$/$A^{2+}2B^{-}$/$2A^{+}B^{2-}$ and $A^{3+}B^{3-}$/$A^{3+}3B^{-}$/$3A^{+}B^{3-}$) of ionic bonds have been investigated. The electrostatic interaction of the $A^{2+}2B^{-}$ (or $2A^{+}B^{2-}$) bond is same with that of the $A^{2+}B^{2-}$ bond along the axial direction. While the electrostatic interaction of the $A^{3+}3B^{-}$ (or $3A^{+}B^{3-}$) bond is same with that of the $A^{3+}B^{3-}$ bond. This study is expected to provide a powerful tool to explore the working mechanism in mechanochemical behaviors of the

double-network polymer composites.

Acknowledgments

This work was financially supported by the National Natural Science Foundation of China (NSFC) under Grant No. 11672342 and 11725208 and Newton Mobility Grant (IE161019) through Royal Society and NFSC.

References

[1] Dopieralski P, Ribas-Arino J, Anjukandi P, Krupicka M, Marx D. Unexpected mechanochemical complexity in the mechanistic scenarios of disulfide bond reduction in alkaline solution. Nat Chem 2017;9:164-70.

[2] Ducrot E, Chen Y, Bulters M, Sijbesma RP, Creton C. Toughening elastomers with sacrificial bonds and watching them break. Science 2014;344:186-9.

[3] Diesendruck CE, Peterson GI, Kulik HJ, Kaitz JA, Mar BD, May PA, White SR, Martínez TJ, Boydston AJ, Moore JS. Mechanically triggered heterolytic unzipping of a low-ceiling-temperature polymer. Nat Chem 2014;6:623-8.

[4] Yoshimoto S, Ohashi F, Kameyama T. Characterization and thermal degradation studies on polyaniline‐intercalated montmorillonite nanocomposites prepared by a solvent‐free mechanochemical route. J Polym Sci Pol Phys 2005;43:2705-14

[5] Lu HB, Liu YZ, Xu BB, Hui D, Fu YQ. Spontaneous biaxial pattern generation and autonomous wetting switching on the surface of gold/shape memory polystyrene bilayer. Compos Part B: Eng 2017;122:9-15.

[6] Bee SL, Abdullah MAA, Mamat M, Bee ST, Sin LT, Hui D, Rahmat AR. Characterization of silylated modified clay nanoparticles and its functionality in PMMA. Compos Part B: Eng 2017;110:83-95.

[7] Javanbakht M, Levitas VI. Phase field simulations of plastic strain-induced phase transformations under high pressure and large shear. Phys Rev B 2016;94:214104.

[8] May PA, Moore JS. Polymer mechanochemistry: techniques to generate molecular force via elongational flows. Chem Soc Rev 2013;42:7497-506.

[9] Church DC, Peterson GI, Boydston AJ. Comparison of mechanochemical chain scission rates for linear versus three-arm star polymers in strong acoustic fields. ACS Macro Lett 2014;3:648-51.

[10] Tran P, Ngo TD, Ghazlan A, Hui D. Bimaterial 3D printing and numerical analysis of bio-inspired composite structures under in-plane and transverse loadings. Compos Part B: Eng 2017;108:210-23.

[11] Sagara Y, Kato T. Mechanically induced luminescence changes in molecular assemblies. Nat Chem 2009;1:605-10.

[12] Wang X, Jiang M, Zhou ZW, Gou JH, Hui D. 3D printing of polymer matrix composites: A review and prospective. Compos Part B: Eng. 2017;110:442-58.

[13] Lu HB, Liu YZ, Huang WM, Wang CC, Hui D, Fu YQ, Controlled evolution of surface patterns for ZnO coated on stretched PMMA upon thermal and solvent treatments. Compos Part B: Eng. 2018;132:1-9.

[14] Sakaguchi M, Yamakawa H, Sohma J. ESR evidence for main‐chain scissions of polypropylene molecules induced by mechanical fracture. J Polym Sci Part C: Polym Lett 1974;12:193-7.

[15] Sasai Y, Yamauchi Y, Kondo SI, Kuzuya M. Nature of mechanoradical formation of substituted celluloses as studied by electron spin resonance Chem Pharm Bull 2004;52:339-44.

[16] Berkowski KL, Potisek SL, Hickenboth CR, Moore JS. Ultrasound-induced site-specific cleavage of azo-functionalized poly (ethylene glycol). Macromolecules 2005;38:8975-8.

[17] Kauzmann WJ, Eyring H. The viscous flow of large molecules. J Am Chem Soc 1940;62:3113-25.

[18] Bell GI. Models for the specific adhesion of cells to cells. Science 1978;200:618-27.

[19] Pipes RB, Pagano NJ. The influence of stacking sequence on laminate strength. J Compos Mater 1970;4:50-7.

[20] Webber RE, Creton C, Brown HR, Gong JP. Large strain hysteresis and mullins effect of tough double-network hydrogels. Macromolecules 2007;40:2919-27.

[21] Jang SS, Goddard WA, Kalani MYS. Mechanical and transport properties of the poly (ethylene oxide)-poly (acrylic acid) double network hydrogel from molecular dynamic simulations. J Phys Chem B 2007;111:1729-37.

[22] Gong JP. Why are double network hydrogels so tough? Soft Matter 2010;6:2583-90.

[23] Gong JP, Katsuyama Y, Kurokawa T, Osada Y. Double-network hydrogels with extremely high mechanical strength. Adv. Mater. 2003;15:1155-8.

[24] Grayson MA, Wolf CJ. Mechanochemical reactions in an epoxy resin system. J Polym Sci Pol Phys 1985;23:1087-97.

[25] Li J, Illeperuma WRK, Suo Z, Vlassak JJ. Hybrid hydrogels with extremely high stiffness and toughness. ACS Macro Lett 2014;3:520-3.

[26] Lu T, Wang J, Yang R, Wang T. A constitutive model for soft materials incorporating viscoelasticity and Mullins effect. J Appl Mech 2017;84:021010.

[27] Marcombe R, Cai S, Hong W, Zhao X, Lapust Y, Suo Z. A theory of constrained swelling of a pH-sensitive hydrogel. Soft Matter 2010;6:784-93.

[28] Yang CH, Wang MX, Haider H, Yang JH, Sun JY, Chen YM, Zhou J, Suo Z. Strengthening alginate/polyacrylamide hydrogels using various multivalent cations. ACS Appl Mater Inter 2013;5:10418-22.

[29] Slutsker AI, Hilyarov VL, Polikarpov I, Karov DD. Possible manifestations of the quantum effect (Tunneling) in elementary events in the fracture kinetics of polymers. Phys Solid State 2010;52:1637-44.

[30] Tomashevskii EE, Egorov EA, Savostin AY. Thermal effects during fracture in polymers. Int J Fracture 1975;11:817-27.

[31] Lu HB, Huang WM, Leng JS. On the origin of Gaussian network theory in the thermo/chemo-responsive shape memory effect of amorphous polymers undergoing photo-elastic transition. Smart Mater Struct 2016;25:065004.

[32] Butyagin PY. Kinetics and nature of mechanochemical reactions. Russ Chem Rev 1971;40:901-15.

[33] Grzemba B. New Experimental investigations on the dieterich-ruina friction law. Facta Universitatis-Series Mechanical Engineering 2015;13:11-20.

[34] Voll L. Experimental investigation of the adhesive contact with elastmoers: effect of surface roughness. Universitatis-Series Mechanical Engineering 2015;13:33-8.

[35] Lantz MA, Hug HJ, Hoffmann R, van Schendel PJA, Kappenberger P, Martin S, Baratoff A, Gu¨ntherodt HJ. Quantitative measurement of short-range chemical bonding forces/ Science 2001;291:2580-3.

[36] Binnig G, Quate CF, Gerber C. Atomic force microscope. Phys Rev Lett 1986;56: 930-4.

[37] Ohnesorge F, Binnig G. True atomic resolution by atomic force microscopy through repulsive and attractive forces. Science 1993;260:1451-6.

[38] Giessibl FJ. Atomic resolution of the silicon (111)-(7x7) surface by atomic force microscopy. Science 1995;267:68-71.

[39] Kitamura S, Iwatsuki M. Observation of 7×7 reconstructed structure on the silicon (111) surface using ultrahigh vacuum noncontact atomic force microscopy. Jpn J Appl Phys 1995;34:145-8.

[40] Grandbois M, Beyer M, Rief M, Clausen-Schaumann H, Gaub HE. How strong is a covalent bond? Science 1999;283:1727-30.

[41] Zhurkov SN, Zakrevskyi VA, Korsukov VE. Mechanism of submicrocrack generation in stressed polymers. J Polym Sci Part A 1972;10:1509-20.

Figure caption

Figure 1. A schematic illustration for the distance of interatomic covalent bond (x) under a force per unit area (f_U) applied on the bond. While the covalent chain is stretched with the macro-force per unit area F. (a) A covalent bond is unstretched with the force per unit area f_U=0. (b) The covalent bond is stretched with the force per unit area f_U>0, resulting in the distance of interatomic covalent bond increased from x to $x+\Delta x$.

Figure 2. Numerical results of the normalized mechanical energy (W_m/D_c) as a function of elongation of the covalent bond (x). (a) Simulation curves for the normalized mechanical energy at different Morse coefficients of α=10^{10}, 2×10^{10}, 3×10^{10}, 4×10^{10} and 5×10^{10}. (b) Simulation curves for the normalized mechanical energy at different dimensionless forces of P=0, 0.2, 0.4, 0.6 and 0.8.

Figure 3. Numerical results of the normalized stress ($S/D_c\alpha$) as a function of bond elongation (x) of the covalent bond. (a) Simulation curves for the normalized stress at different Morse coefficients of α=10^{10}, 2×10^{10}, 3×10^{10}, 4×10^{10} or 5×10^{10}. (b) Simulation curves for the normalized stress at different dimensionless forces of P=0, 0.2, 0.4, 0.6 and 0.8.

Figure 4. Numerical results of the mechanical energy (W_e/ke^2) for electrostatic force as a function of interatomic distance of the scission bond (x) and Morse potential constant (α_i) for the ionic bond. (a) Simulation curves for the mechanical energy (W_e/ke^2) for electrostatic force at a given constant of $\alpha_i r$=4, 5, 8 and 10. (b) Simulation curves for the mechanical energy (W_e/ke^2) for electrostatic force at a given constant of R/r=1.01, 1.05, 1.2 and 2.0.

Figure 5. (a) The electrostatic interaction for the $A^{2+}2B^{-}$ (or $2A^{+}B^{2-}$) ionic bond. (b) The electrostatic interaction for the $A^{3+}3B^{-}$ (or $3A^{+}B^{3-}$) ionic bond.

Figure 6. Numerical results of the mechanical energy for electrostatic force of the $A^{2+}B^{2-}$ ($A^{2+}2B^{-}$ or $2A^{+}B^{2-}$) and $A^{3+}B^{3-}$ ($A^{3+}3B^{-}$ or $3A^{+}B^{3-}$) ionic bond. (a) Simulation results of the mechanical energy (W_e/ke^2) as a function of elongation of the ionic bond (x). (b) Simulation results of the mechanical energy (W_e/ke^2) as a function of Morse potential constant (α_i).

Figure 7. Numerical results of the mechanical energy (W) and deformation mechanical energy (W_m) as a function of the covalent/ionic bond elongation ($x_c = x_i = x$, where x_c and x_i are the elongation of the covalent bond and ionic bond, respectively.). At a given Morse potential constant of (a) $\alpha = 10^{10}$. (b) $\alpha = 1.25\times10^{10}$. (c) $\alpha = 1.6\times10^{10}$. (d) $\alpha = 2\times10^{10}$.

Figure 8. (a) Numerical results of the deformation mechanical energy (W_m) against elongation of the covalent/ionic bond (x) at given Morse potential constants of $\alpha = 10^{10}$, $\alpha = 1.25\times10^{10}$, $\alpha = 1.6\times10^{10}$ and $\alpha = 2\times10^{10}$. (b) Numerical results of the polar mechanical energy (W_e) against elongation of the covalent/ionic bond (x) at given Morse potential constants of $\alpha = 10^{10}$, $\alpha = 1.25\times10^{10}$, $\alpha = 1.6\times10^{10}$ to $\alpha = 2\times10^{10}$.

Figure 9. A divergence of the mechanical energy for deformation of the covalent and ionic bonds as a function of the elongation of covalent (or ionic) bond at given ionic bond numbers of $\alpha = 10^{10}$, $\alpha = 1.25\times10^{10}$, $\alpha = 1.6\times10^{10}$ and $\alpha = 2\times10^{10}$.

Figure 10. The constitutive relationship of the mechanical stress as a function of the elongation of covalent (or ionic) bond at a given Morse potential constant of (a) $\alpha_i = \alpha_c = 10^{10}$ and $\alpha_i = \alpha_c = 1.25\times10^{10}$. (b) $\alpha_i = \alpha_c = 1.6\times10^{10}$ and $\alpha_i = \alpha_c = 2\times10^{10}$.

Figure 11. (a) The constitutive relationship of the dissociation energy of the interatomic ionic bond (D_i) as a function of the Morse coefficient α_i (α_i is also assumed to the bond number of the ionic network). (b) The constitutive relationship of the maximum force under static

elastic tension of the ionic bond (P_i=1 and $f_U = F_m$) as a function of the Morse coefficient α_i.

Figure 12. The constitutive relationship of the mechanical stress as a function of the covalent (or ionic) bond elongation. (a) At different Morse potential constants of $\alpha_i = \alpha_c$=10^{10} and $\alpha_i = \alpha_c$=1.25×10^{10}. (b) Difference of the deformation force for the covalent network in comparison with that of the double-network at various Morse potential constants of $\alpha_i = \alpha_c$ =10^{10} and $\alpha_i = \alpha_c$ =1.25×10^{10}. (c) At different Morse potential constants of $\alpha_i = \alpha_c$=1.6×10^{10} and $\alpha_i = \alpha_c$=2×10^{10}. (d) Changes of the deformation force for the covalent network in comparison with that of the double-network at various Morse potential constants of $\alpha_i = \alpha_c$=1.6×10^{10} and $\alpha_i = \alpha_c$=2×10^{10}.

Figure 13. (a) The simulation curves of energy-elongation contrast with the experiment data [35]. (b) Divergence of simulation and experimental results of energy. (c) The simulation curves of stress-elongation contrast with the experiment data [40]. (d) Divergence of simulation and experimental results of stress. The dot implicates the experiment data.

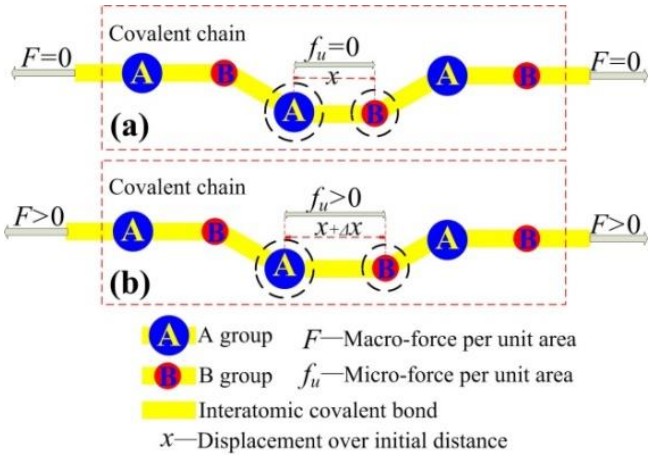

Figure 1. A schematic illustration for the distance of interatomic covalent bond (x) under a force per unit area (f_U) applied on the bond. While the covalent chain is stretched with the macro-force per unit area F. (a) A covalent bond is unstretched with the force per unit area f_U=0. (b) The covalent bond is stretched with the force per unit area f_U>0, resulting in the distance of interatomic covalent bond increased from x to $x+\Delta x$.

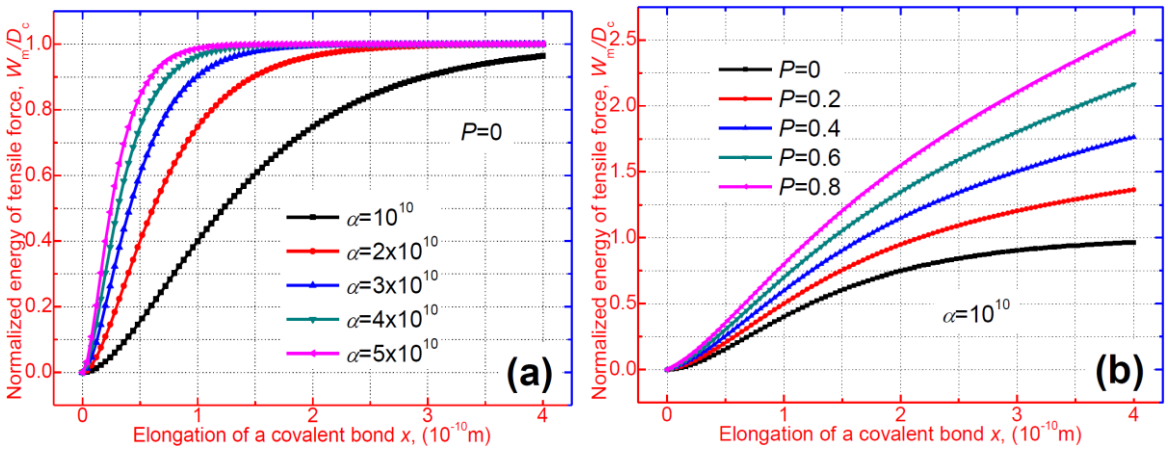

Figure 2. Numerical results of the normalized mechanical energy (W_m/D_c) as a function of elongation of the covalent bond (x). (a) Simulation curves for the normalized mechanical energy at different Morse coefficients of α=10^{10}, 2×10^{10}, 3×10^{10}, 4×10^{10} and 5×10^{10}. (b) Simulation curves for the normalized mechanical energy at different dimensionless forces of P=0, 0.2, 0.4, 0.6 and 0.8.

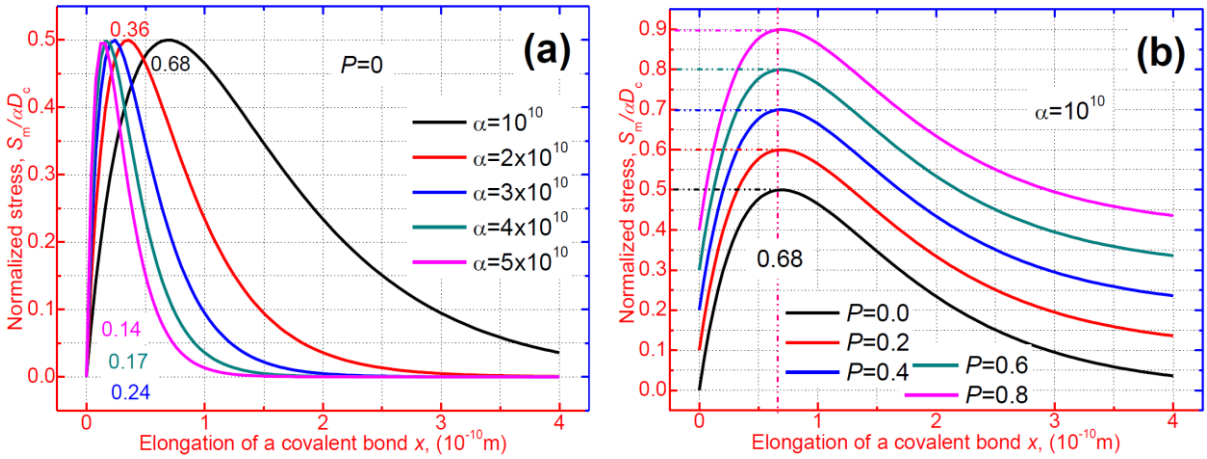

Figure 3. Numerical results of the normalized stress ($S/D_c\alpha$) as a function of bond elongation (x) of the covalent bond. (a) Simulation curves for the normalized stress at different Morse coefficients of α =10^{10}, 2×10^{10}, 3×10^{10}, 4×10^{10} or 5×10^{10}. (b) Simulation curves for the normalized stress at different dimensionless forces of P =0, 0.2, 0.4, 0.6 and 0.8.

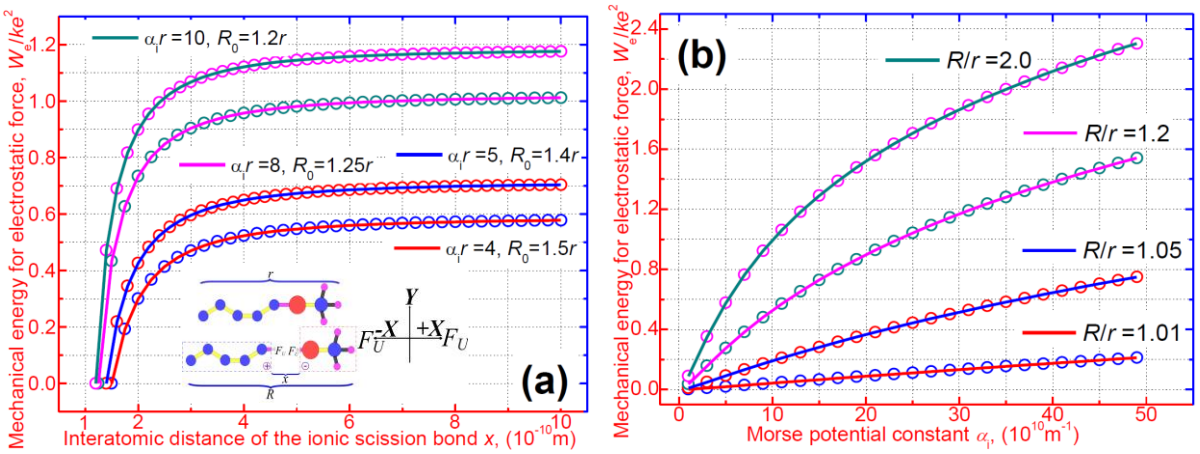

Figure 4. Numerical results of the mechanical energy (W_e/ke^2) for electrostatic force as a function of interatomic distance of the scission bond (x) and Morse potential constant (α_i) for the ionic bond. (a) Simulation curves for the mechanical energy (W_e/ke^2) for electrostatic force at a given constant of $\alpha_i r$ =4, 5, 8 and 10. (b) Simulation curves for the mechanical energy (W_e/ke^2) for electrostatic force at a given constant of R/r =1.01, 1.05, 1.2 and 2.0.

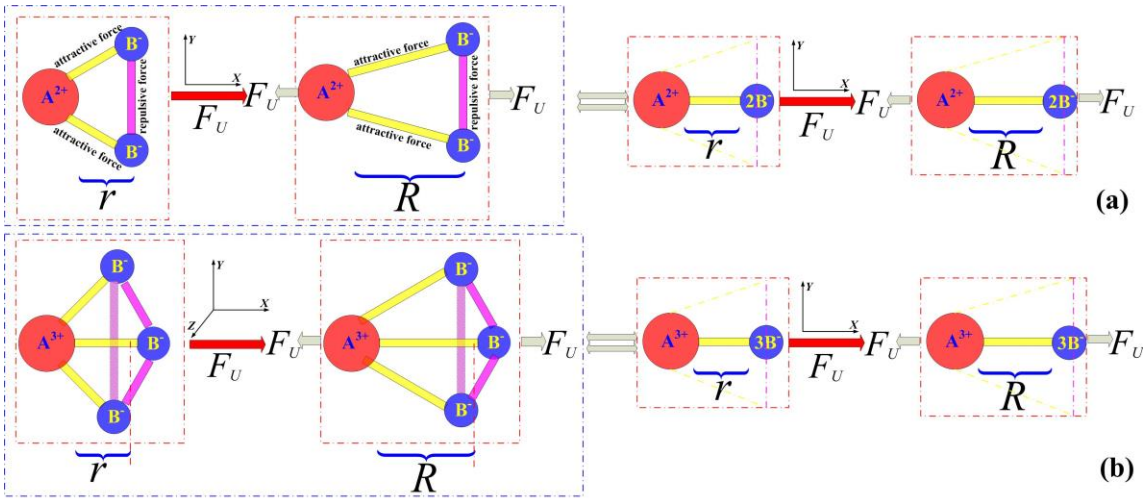

Figure 5. (a) The electrostatic interaction for the $A^{2+}2B^-$ (or $2A^+B^{2-}$) ionic bond. (b) The electrostatic interaction for the $A^{3+}3B^-$ (or $3A^+B^{3-}$) ionic bond.

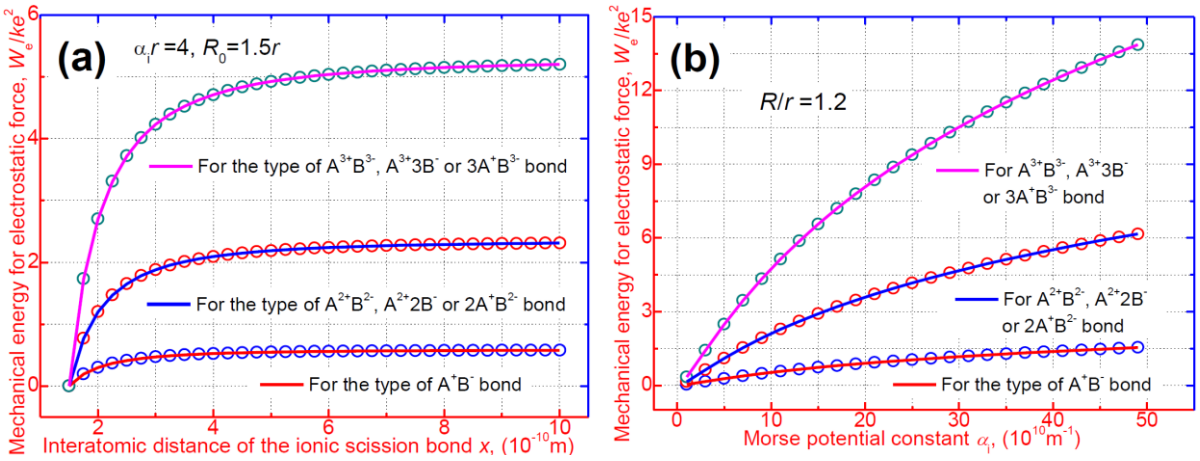

Figure 6. Numerical results of the mechanical energy for electrostatic force of the $A^{2+}B^{2-}$ ($A^{2+}2B^{-}$ or $2A^{+}B^{2-}$) and $A^{3+}B^{3-}$ ($A^{3+}3B^{-}$ or $3A^{+}B^{3-}$) ionic bond. (a) Simulation results of the mechanical energy (W_e/ke^2) as a function of elongation of the ionic bond (x). (b) Simulation results of the mechanical energy (W_e/ke^2) as a function of Morse potential constant (α_i).

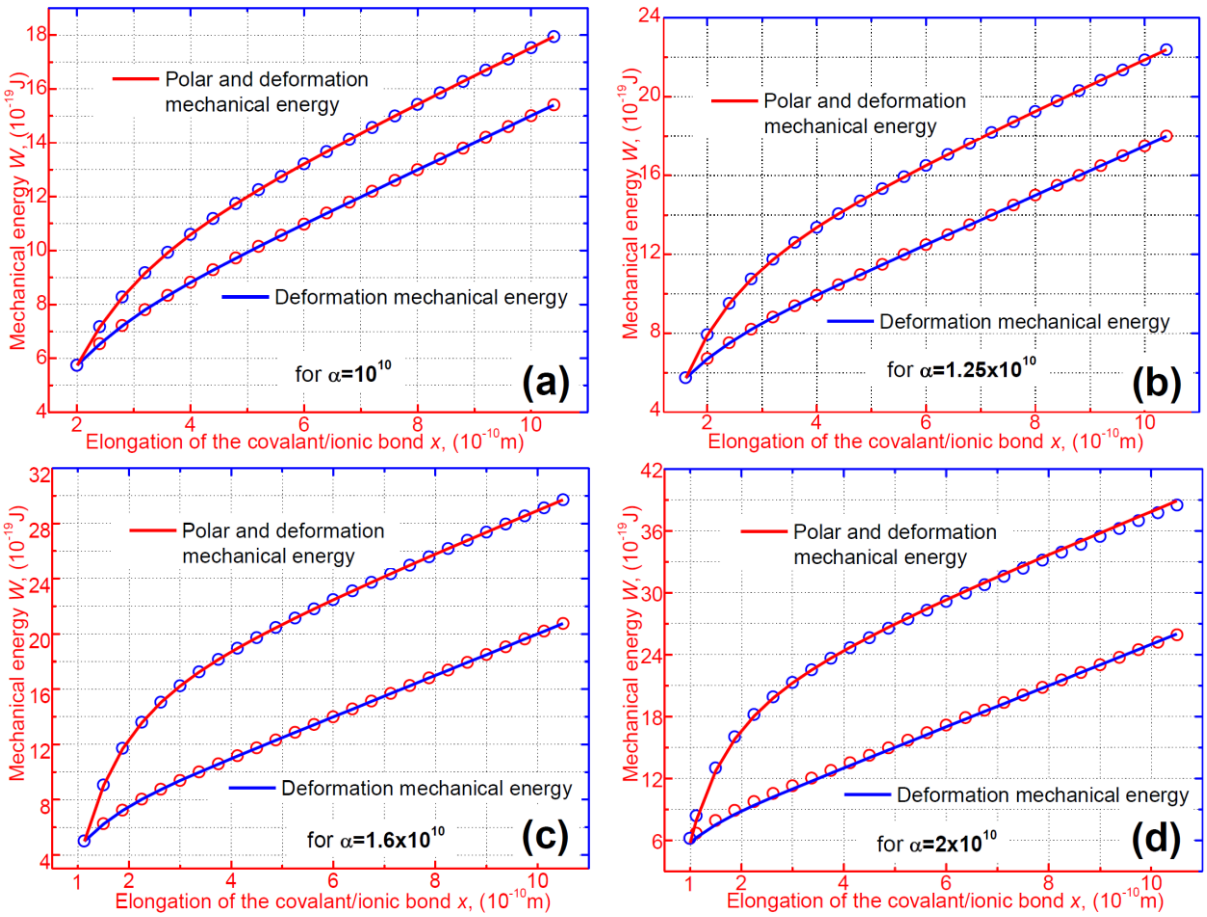

Figure 7. Numerical results of the mechanical energy (W) and deformation mechanical energy (W_m) as a function of the covalent/ionic bond elongation ($x_c = x_i = x$, where x_c and x_i are the elongation of the covalent bond and ionic bond, respectively.). At a given Morse potential constant of (a) $\alpha = 10^{10}$. (b) $\alpha = 1.25\times10^{10}$. (c) $\alpha = 1.6\times10^{10}$. (d) $\alpha = 2\times10^{10}$.

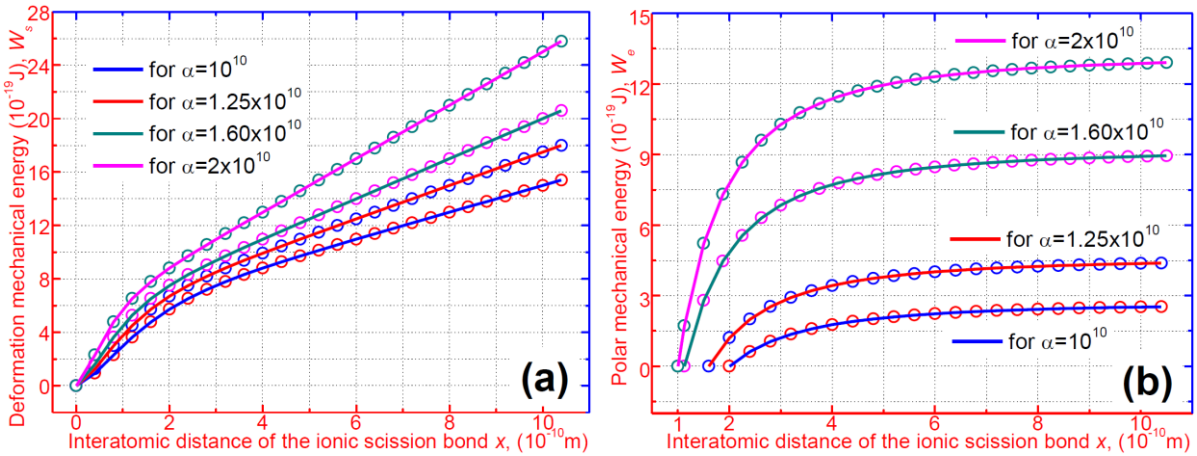

Figure 8. (a) Numerical results of the deformation mechanical energy (W_m) against elongation of the covalent/ionic bond (x) at given Morse potential constants of α=10^{10}, α=1.25×10^{10}, α=1.6×10^{10} and α=2×10^{10}. (b) Numerical results of the polar mechanical energy (W_e) against elongation of the covalent/ionic bond (x) at given Morse potential constants of α=10^{10}, α=1.25×10^{10}, α=1.6×10^{10} to α=2×10^{10}.

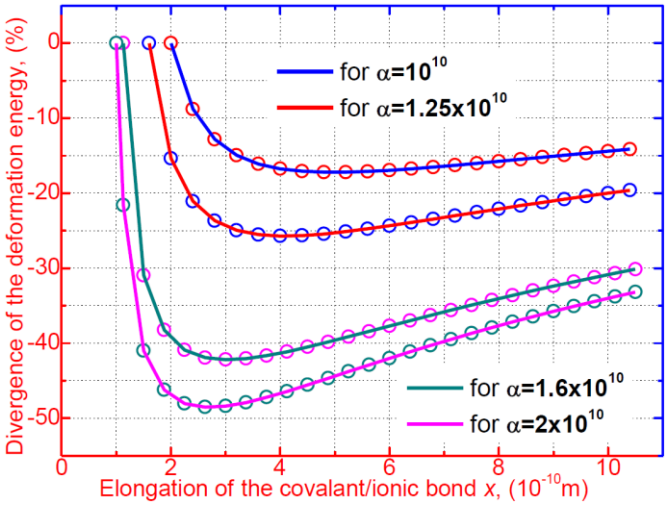

Figure 9. A divergence of the mechanical energy for deformation of the covalent and ionic bonds as a function of the elongation of covalent (or ionic) bond at given ionic bond numbers of $\alpha = 10^{10}$, $\alpha = 1.25\times10^{10}$, $\alpha = 1.6\times10^{10}$ and $\alpha = 2\times10^{10}$.

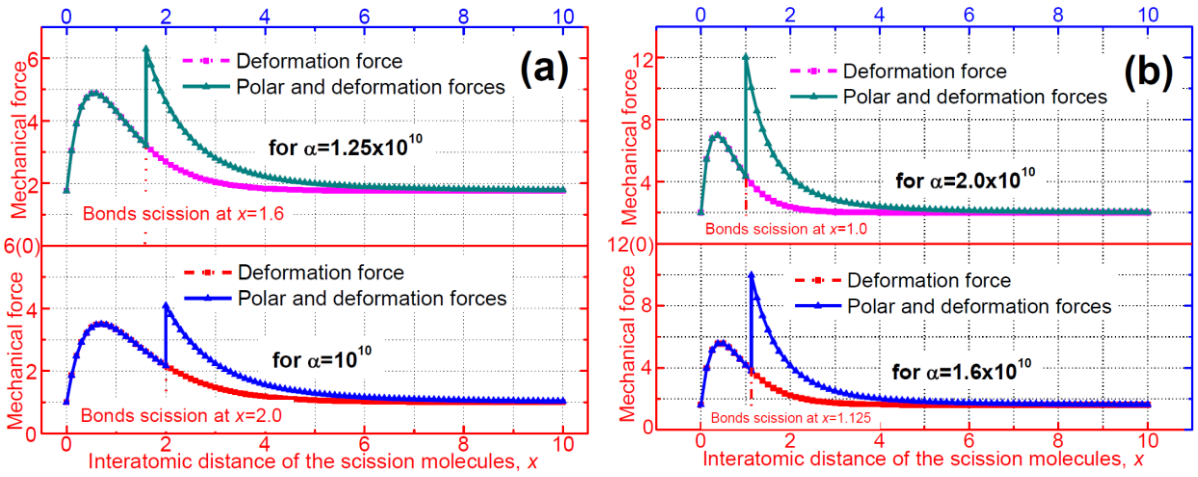

Figure 10. The constitutive relationship of the mechanical stress as a function of the elongation of covalent (or ionic) bond at a given Morse potential constant of (a) $\alpha_i = \alpha_c = 10^{10}$ and $\alpha_i = \alpha_c = 1.25\times10^{10}$. (b) $\alpha_i = \alpha_c = 1.6\times10^{10}$ and $\alpha_i = \alpha_c = 2\times10^{10}$.

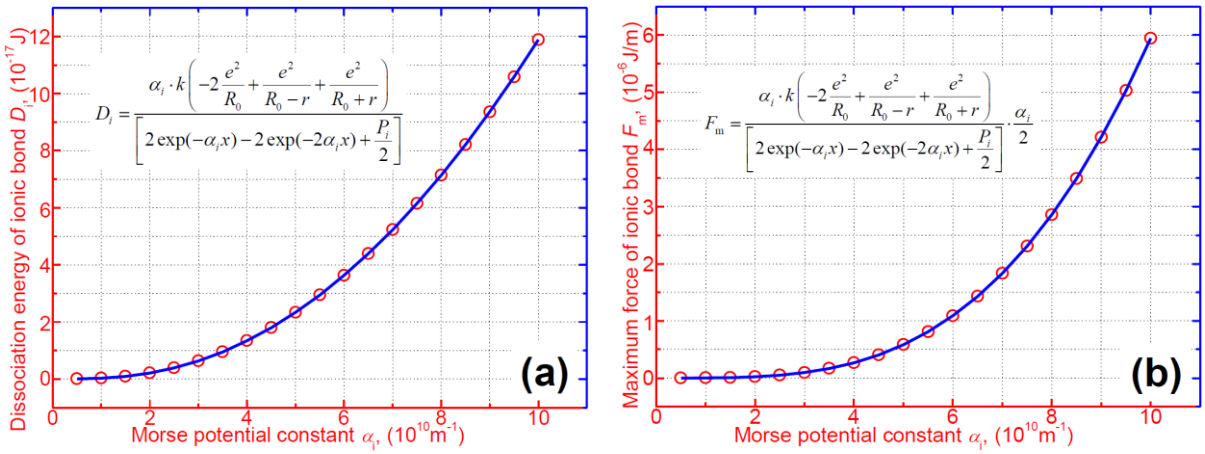

Figure 11. (a) The constitutive relationship of the dissociation energy of the interatomic ionic bond (D_i) as a function of the Morse coefficient α_i (α_i is also assumed to the bond number of the ionic network). (b) The constitutive relationship of the maximum force under static elastic tension of the ionic bond (P_i =1 and $f_U = F_m$) as a function of the Morse coefficient α_i.

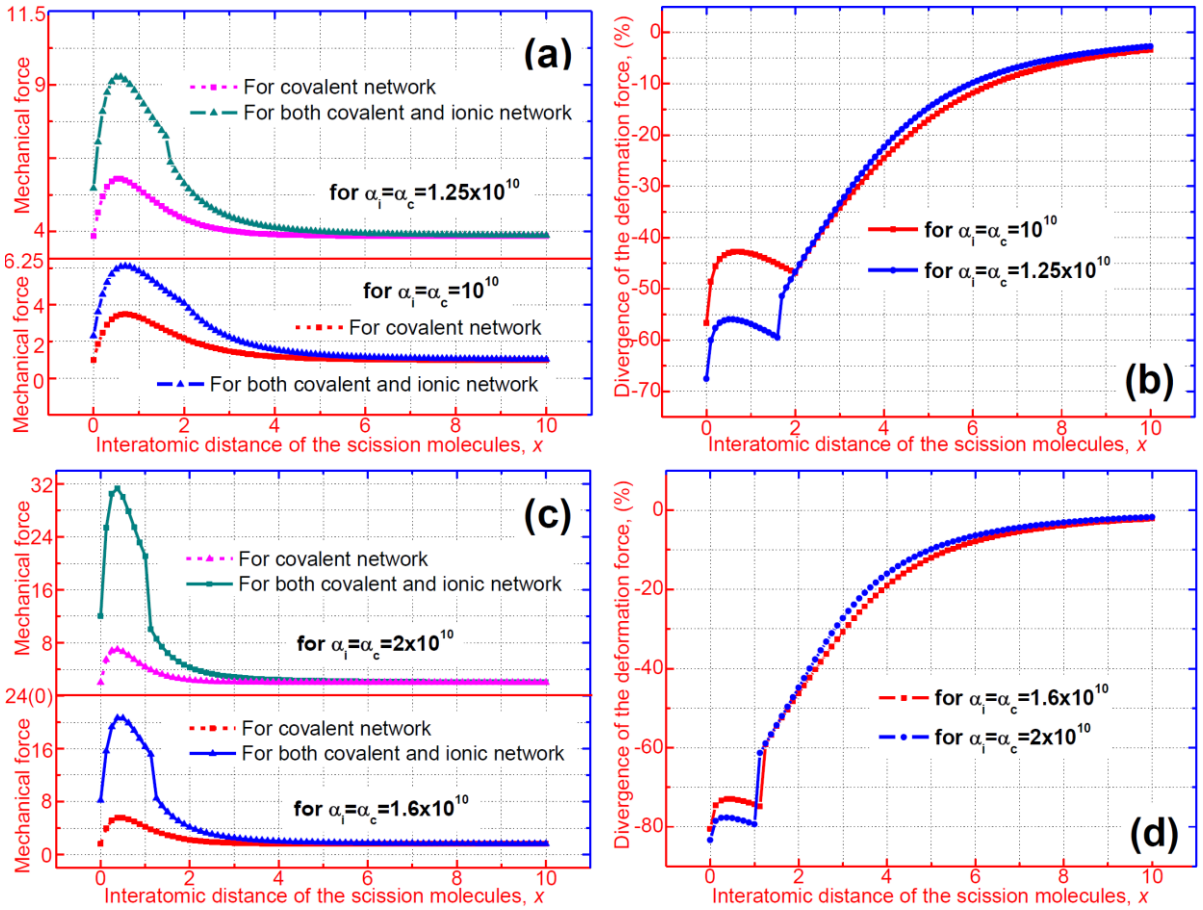

Figure 12. The constitutive relationship of the mechanical stress as a function of the covalent (or ionic) bond elongation. (a) At different Morse potential constants of $\alpha_i=\alpha_c=10^{10}$ and $\alpha_i=\alpha_c=1.25\times10^{10}$. (b) Difference of the deformation force for the covalent network in comparison with that of the double-network at various Morse potential constants of $\alpha_i=\alpha_c=10^{10}$ and $\alpha_i=\alpha_c=1.25\times10^{10}$. (c) At different Morse potential constants of $\alpha_i=\alpha_c=1.6\times10^{10}$ and $\alpha_i=\alpha_c=2\times10^{10}$. (d) Changes of the deformation force for the covalent network in comparison with that of the double-network at various Morse potential constants of $\alpha_i=\alpha_c=1.6\times10^{10}$ and $\alpha_i=\alpha_c=2\times10^{10}$.

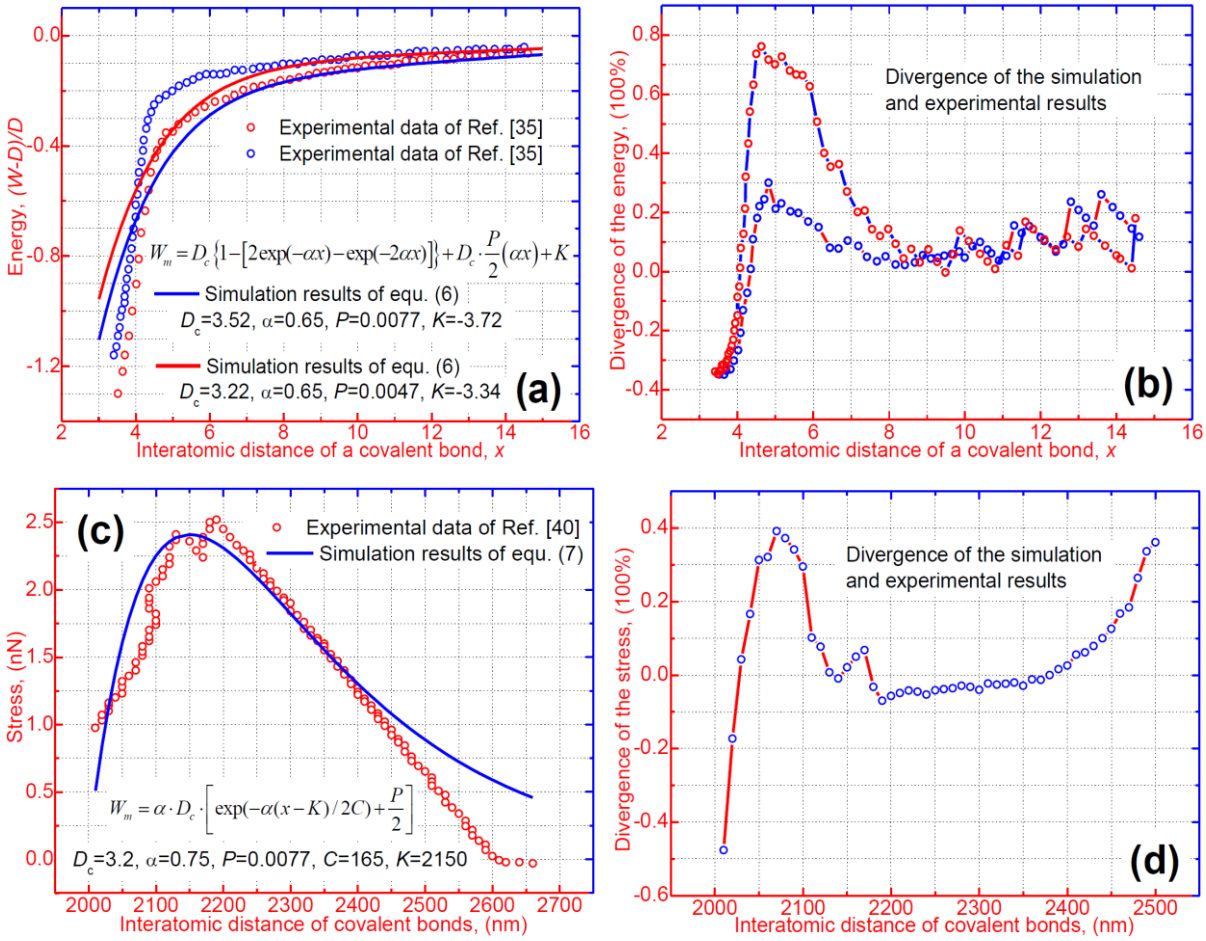

Figure 13. (a) The simulation curves of energy-elongation contrast with the experiment data [35]. (b) Divergence of simulation and experimental results of energy. (c) The simulation curves of stress-elongation contrast with the experiment data [40]. (d) Divergence of simulation and experimental results of stress. The dot implicates the experiment data.